Brittle and ductile friction and the physics of tectonic tremor

Eric G. Daub[1,2], David R. Shelly[3], Robert A. Guyer[1,4], and Paul A. Johnson[1]

1. Geophysics Group, Los Alamos National Laboratory
2. Center for Nonlinear Studies, Los Alamos National Laboratory
3. United States Geological Survey, Menlo Park
4. Department of Physics, University of Nevada, Reno

Summary: A model for brittle and ductile friction, combined with seismic observations, captures the dynamics of tectonic tremor and produces all types of fault slip, including earthquakes, tremor, transient silent slip, and steady creep.

Abstract

Observations of nonvolcanic tremor provide a unique window into the mechanisms of deformation and failure in the lower crust. At increasing depths, rock deformation gradually transitions from brittle, where earthquakes occur, to ductile, with seismic tremor occurring in the transitional region. We show that a physical model that combines both brittle and ductile deformation captures observations of tremor dynamics at Parkfield and provides constraints on

the friction and stress in the lower crust. Our results show that tremor occurs over a range of values but requires a balance between brittle and ductile processes, which advances our understanding of the basic physics of tremor and earthquakes.

The occurrence of earthquakes in the upper ~ 15 km of the crust (known as the seismogenic zone) indicates that the rocks in the upper crust are usually brittle and resist the slow deformation of tectonic plate motion. With increasing depth and increasing temperature, the mechanical properties gradually transition from brittle to ductile. Ductile fault rocks creep steadily with plate motion rather than failing suddenly as earthquakes. Recent observations show that deformation in the brittle-ductile transition region often occurs transiently and is observed seismically as non-volcanic tremor and low frequency earthquakes (LFEs) [1, 2, 3, 4], and geodetically as silent slip events [5, 6]. Tremor and silent slip occur in many different tectonic regimes, and provide important clues into the nature of fault slip at depth.

While many studies have examined the brittle-ductile transition in laboratory rock specimens [7, 8], the lack of observational constraints make it difficult to determine exactly how this transition occurs in Earth. Modeling studies have focused on transient slip in the lower crust (e.g. [9, 10]), but the physics that produces the range of fault slip behaviors observed at depth remains poorly understood. By combining insight from laboratory experiments with seismic observations, we construct a model for slip and failure at depth, providing new insight into the dynamics of Earth's crust.

Figure 1(a) shows a side view of the San Andreas Fault at Parkfield. The upper

~ 15 km comprises the seismogenic zone, where the fault is brittle and earthquakes occur. Below ~ 15 km depth, the frictional properties begin to change from brittle to ductile, where LFEs and tremor events occur.

LFEs are located by identifying P and S wave arrivals on stacked seismic waveforms [12]. Once an event is located, additional occurrences of this event are identified by a cross correlation of the tremor waveforms with the seismic data at multiple 3-component stations at Parkfield [13, 14]. The set of repeated occurrences are referred to as a "family," and each family represents a repeating LFE at a single spatial location. The LFE bursts show a rich variety of dynamics, including two period recurrence intervals [15], complex migration along strike [16], and temporal changes in activity associated with the 2004 Parkfield earthquake [15, 17].

To characterize the observations, we develop a model to capture the dynamics of an LFE family and deduce the physical mechanisms of fault slip at depth. We approximate the slipping patch at depth corresponding to a single family as a block slider, as shown in Figure 1(b). The block of mass m is attached to a spring of stiffness Γ, and the spring is pulled at a constant velocity V_0. The driving velocity V_0 corresponds to the long-term slip rate on the San Andreas Fault, constrained through geodetic measurements to be about 30 mm/year [18].

The block motion is resisted by friction that is both brittle and ductile. The brittle part of the friction is the sum over a series of frictional contacts [19], which resist motion and fail suddenly, as illustrated in Figure 1(c). An idealized frictional contact forms at a position x_{0i} (left) and exerts a stress proportional to the relative displacement of the surfaces with stiffness γ (center). When the displacement is larger than some failure distance a_i, the contact breaks and a new contact forms.

The contact failure distances a_i are drawn from a probability distribution $p_0(a) \propto a^{-2}$, which reflects the roughness of the sliding interfaces. This distribution is consistent with laboratory experiments that measured asperity contact diameters of roughened surfaces [20], and with field observations of natural faults that show that gouge particle diameters are power law distributed [21].

The ductile part of the friction damps the motion of the block. The ductile shear stress increases with the logarithm of the relative velocities of the surfaces, consistent with laboratory friction experiments [22], with an overall strength σ_d.

The equations of motion for the block are

$$\frac{m}{A}\frac{dV}{dt} = \Gamma\left(V_0 t - x\right) - \sum_{i=1}^{N_c} \gamma\left(x - x_{0i}\right) - \sigma_d \log\left(\frac{V + V_0}{V_0}\right) - \frac{\mu}{2c_s}V; \tag{1}$$

$$\frac{dx}{dt} = V. \tag{2}$$

The first equation is Newton's second law divided by the fault area A so that the frictional terms are expressed in terms of shear stress rather than force. The first term on the right hand side of Equation (1) is the shear stress exerted by the spring (the advancing tectonic plate), the second term is friction due to brittle contacts at the fault interface, the third term is the friction due to ductile contacts at the fault interface, and the last term is radiation damping, damping due to energy loss to seismic radiation, where μ is the shear modulus and c_s is the shear wave speed. Parameter values and additional model details are described in the supplementary material.

Figure 2(a) shows an example of the shear stress exerted by the spring as a function of time. The block undergoes stick-slip motion, with stress drops of order 10 kPa. The stress drops are of the same order of magnitude as tidal stresses, which were shown to correlate with tremor activity at Parkfield [23]. Figure 2(b) shows that each slip event consists of several individual LFEs. Each individual event consists of a collection of frictional contacts failing, corresponding to a patch slipping on the fault. This matches observations of bursts of LFEs at Parkfield. An example of LFE activity recorded at the surface at Parkfield is shown in Figure 2(c). Circles at the top of the plot show detected events, with different colors corresponding to various LFE families. Note that during the burst, LFEs from a given family occur multiple times, as in the model.

Without the ductile damping, which slows the block, the model produces earthquakes where the slip occurs in a single event rather than in bursts. Bursts of activity are a common feature of tremor [24], which indicates that our results are applicable to tremor in many tectonic settings.

Seismic observations show that both the recurrence time between bursts and the burst duration vary with the LFE family. In the model, the recurrence time increases with increasing brittle contact strength, as the stress drop is larger and more time is required for tectonic loading to bring the stress to the point of failure. Recurrence time also increases as the ductile strength decreases, due to increased dynamic overshoot of the slip of the block relative to the loading point displacement. Interevent recurrence time is also dependent on the spring stiffness – a more compliant spring leads to longer recurrence times. LFE burst duration is dependent on both the brittle and the ductile strengths. Longer bursts occur for increased brittle strength, as the recurrence time is larger and more slip occurs during each event. Larger ductile damping strength leads to longer bursts by reducing the slip rate during failure.

To deduce the range of frictional properties *in situ*, we perform a systematic study of the dynamics as a function of the strength of the brittle and ductile components in the model. At a given value of the brittle contact stiffness, earthquakes occur for weak ductile damping, tremor occurs for intermediate ductile damping, and steady sliding occurs for strong ductile damping. We identify the transition from earthquakes to tremor by identifying parameters that produce slip events with a single peak in the slip rate (earthquakes), rather than a burst with multiple peaks (tremor, Fig. 2(b)). Steady sliding occurs when the slip rate is maintained within an order of magnitude of the driving rate V_0. Between these regimes, we see a range of tremor dynamics. Based on the seismic data, we estimate a lower bound of 10^{-4} m/s on the slip rate during LFEs (details in the supplementary material). We classify events with slip rates below 10^{-4} m/s as silent slip events, and we classify events with slip rates above 10^{-4} m/s as LFEs/tremor.

Figure 3(a) shows a phase diagram of the model dynamics as a function of the total brittle contact strength (the time average of the sum over all brittle contact stresses) and the ductile damping strength σ_d. The diagram illustrates that a range of parameters lead to LFEs. Within the LFE regime, tighter constraints on the parameters can be obtained by using recurrence time and burst duration to determine the specific values of the brittle and ductile strengths. For LFEs with recurrence times of ~ 3 days, the model produces similar dynamics to the observations with a brittle strength of 1 MPa, and a ductile damping strength of $\sigma_d = 0.007$ MPa. For LFE families with longer recurrence times, both the brittle and ductile strengths are larger.

Figure 3(b) shows the phase diagram in Figure 3(a), with the axes transformed to show the effective normal stress on the fault, and the fraction of contacts that are brittle. The transformation assumes that the brittle friction has a friction coefficient of 0.7, and that the ductile damping strength is proportional to the normal stress by a factor of 0.01, based on laboratory experiments [22]. Our model shows that LFEs only occur if the fraction of contacts that are brittle is between 0.4-0.7, independent of the normal stress. For LFEs with recurrence times of ~ 3 days, the fraction of contacts that are brittle is 0.67, and the effective normal stress is very low, 2.13 MPa. This suggests that the effective stress is low at tremor locations with short recurrence times. Similar values of the fraction of contacts that are brittle and higher values of the normal stress result in LFE families with longer recurrence times and longer burst durations. Tremor at shallower depths tends to have longer recurrence times [16], suggesting that pore pressure is greater at large depths.

Our model shows that for observable tremor to occur, 40%-70% of the minerals in fault rocks must be brittle at depth. Quartz and feldspar are the most abundant minerals in the crust [25], and at Parkfield, the relative amounts of quartz and feldspar vary spatially [26]. Field observations of exhumed strike-slip faults show evidence of brittle deformation of feldspar at the same depths as ductile deformation of quartz [27]. Additionally, laboratory studies show that quartz begins to deform in a ductile manner at a lower temperature than feldspar [28]. Relative variations in the amount of quartz and feldspar at different spatial locations could be responsible for the diverse tremor dynamics observed at Parkfield. The results also suggest that below the rupture segment of the 2004 Parkfield earthquake where no tremor has been observed (Fig. 1(a)), $\sim$40% or less of contacts are deforming in a brittle manner.

Our results have important implications for seismic hazard. Most models of the seismic cycle use the laboratory derived rate and state friction laws (e.g. [29, 30]) that do not capture the combination of brittle and ductile processes in our model. Deformation in the lower crust may precede earthquake nucleation in the seismogenic zone [17]. Our model provides constraints on the frictional properties at depth, and could provide additional clues as to how deformation in the lower crust is related to damaging earthquakes in the upper crust in many different tectonic settings.

References

[1] K. Obara, Nonvolcanic deep tremor associated with subduction in southwest Japan. *Science* **296**, 1679-1681 (2002).

[2] G. Rogers, H. Dragert, Episodic Tremor and Slip on the Cascadia Subduction Zone: The Chatter of Silent Slip. *Science* **300**, 5627, 1942-1943 (2003).

[3] A. Katsumata, N. Kamaya. Low-frequency continuous tremor around the Moho discontinuity away from volcanoes in the southwest Japan. *Geophys. Res. Lett.* **30** (2003).

[4] D. R. Shelly, G. C. Beroza, S. Ide, S. Nakamula. Low-frequency earthquakes in Shikoku, Japan and their relationship to episodic tremor and slip. *Nature* **442**, 188191 (2006).

[5] H. Dragert, K. Wang, T. S. James, A Silent Slip Event on the Deeper Cascadia Subduction Interface. *Science* **292**, 5521, 1525-1528 (2001).

[6] H. Hirose, K. Hirahara, F. Kimata, N. Fujii, S. Miyazaki, A slow thrust slip event following the two 1996 Hyuganada Earthquakes beneath the Bungo Channel, southwest Japan. *Geophys. Res. Lett.* **26(21)**, 3237-3240 (1999).

[7] R. M. Stesky, W. F. Brace, D. K. Riley, P. Y. F. Robin, Friction in faulted rock at high temperature and pressure. *Tectonophysics* **23(12)**, 177203 (1974).

[8] B. Evans, J. T. Fredrich, T.-F. Wong, in *The Brittle-Ductile Transition in Rocks*, *Geophysical Monograph* **56** (AGU, Washington, D.C., 1990) pp. 1-20.

[9] Y. Liu, J. R. Rice, Spontaneous and triggered aseismic deformation transients in a subduction fault model. *J. Geophys. Res.* **112**, B09404 (2007).

[10] R. Ando, R. Nakata, T. Hori, A slip pulse model with fault heterogeneity for low-frequency earthquakes and tremor along plate interfaces. *Geophys. Res. Lett.* **37**, L10310 (2010).

[11] F. Waldhauser, D. P. Schaff, Large-scale relocation of two decades of northern California seismicity using cross-correlation and double-difference methods. *J. Geophys. Res.* **113**, B08311 (2008).

[12] D. R. Shelly, J. L. Hardebeck, Precise tremor source locations and amplitude variations along the lower-crustal central San Andreas Fault. *Geophys. Res. Lett.* **37**, L14301 (2010).

[13] D. R. Shelly, G. C. Beroza, S. Ide, Non-volcanic tremor and low frequency earthquake swarms. *Nature* **446**, 305307 (2007).

[14] D. R. Shelly, *et al.* Precise location of San Andreas Fault tremors near Cholame, California using seismometer clusters: Slip on the deep extension of the fault? Geophys. Res. Lett. **36**, L01303 (2009).

[15] D. R. Shelly, Periodic, chaotic, and doubled earthquake recurrence intervals on the deep San Andreas Fault. *Science* **328**, 1385-1388 (2010).

[16] D. R. Shelly, Migrating tremors illuminate complex deformation beneath the seismogenic San Andreas fault. *Nature* **463**, 648-652 (2010).

[17] D. R. Shelly, Possible deep fault slip preceding the 2004 Parkfield earthquake, inferred from detailed observations of tectonic tremor. *Geophys. Res. Lett.* **36**, L17318 (2009).

[18] J. Murray, J. Langbein, Slip on the San Andreas Fault at Parkfield, California, over Two Earthquake Cycles, and the Implications for Seismic Hazard. *Bull. Seismol. Soc. Am.* **96(4B)**, S283-S303 (2006).

[19] R. A. Guyer, paper presented at the 13th Annual International Conference on Nonliner Elastic Materials, Aix en Provence, France, 2008.

[20] J. H. Dieterich, B. D. Kilgore, Imaging surface contacts: power law contact distributions and contact stresses in quartz, calcite, glass and acrylic plastic. *Tectonophys.* **256(1-4)**, 219-239 (1996).

[21] J. S. Chester, F. M. Chester, A. K. Kronenberg, Fracture surface energy of the Punchbowl fault, San Andreas system. *Nature* **437**, 133-136 (2005).

[22] M. L. Blanpied, D. A. Lockner, J. D. Byerlee, Frictional slip of granite at hydrothermal conditions. *J. Geophys. Res.* **100(B7)**, 13045-13064 (1995).

[23] A. M. Thomas, R. M. Nadeau, R. Bürgmann, Tremor-tide correlations and near-lithostatic pore pressure on the deep San Andreas fault. *Nature* **462**, 1048-1051 (2009).

[24] S. Ide, G. C. Beroza, D. R. Shelly, T. Uchide, A scaling law for slow earthquakes. *Nature* **447**, 76-79 (2007).

[25] R. L. Rudnick, S. Gao, in *The Crust*, *Treatise on Geochemistry* **3**, ed. R. L. Rudnick (Elsevier-Pergamon, Oxford, 2003) pp. 1-64.

[26] J. G. Solum *et al.* Mineralogical characterization of protolith and fault rocks from the SAFOD Main Hole. *Geophys. Res. Lett.* **33**, L21314 (2006).

[27] J. Cole *et al.* Localized ductile shear below the seismogenic zone: Structural analysis of an exhumed strike-slip fault, Austrian Alps. *J. Geophys. Res.* **112**, B12304 (2007).

[28] C. H. Scholz, The brittle-plastic transition and the depth of seismic faulting. *Geol. Rund.* **77**, 319-328 (1988).

[29] N. Lapusta, J. R. Rice, Y. Ben-Zion, G. Zheng, Elastodynamic analysis for slow tectonic loading with spontaneous rupture episodes on faults with rate- and state-dependent friction. *J. Geophys. Res.* **105(B10)**, 23765-23789 (2000).

[30] J. H. Dieterich, K. B. Richards-Dinger, Earthquake recurrence in simulated fault systems. *Pure Appl. Geophys.*, in press.

[31] We thank Fred Pollitz and James Savage for helpful reviews. This work was supported by institutional LDRD funding at Los Alamos.

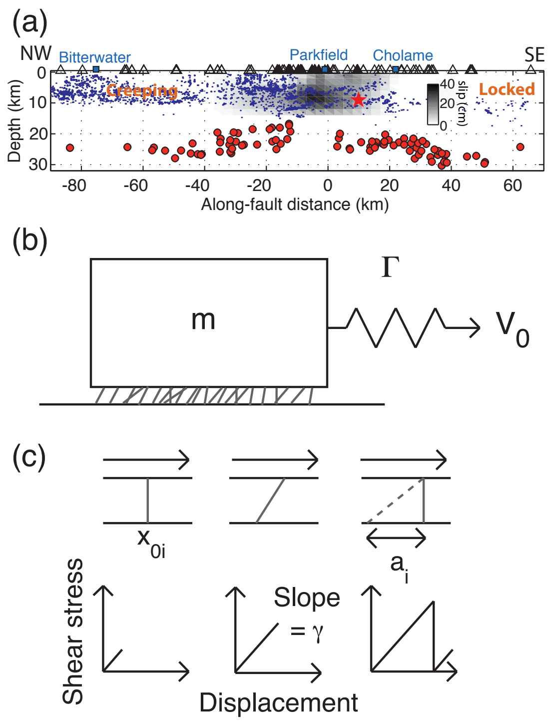

Figure 1: (a) Side view of the San Andreas Fault at Parkfield. At depths up to ~ 15 km, fault slip occurs as earthquakes. Shading shows the fault slip in the 2004 Parkfield earthquake with the hypocenter indicated by the star, and the small dots indicate seismicity within 5 km of the fault [11]. At greater depths, tremor occurs, with the larger circles denoting LFE locations. Figure adapted from ref. [12]. (b) Top view of the simple faulting model for tremor. Tremor at a single location is modeled as a rigid block pulled across a rough surface by a spring of stiffness Γ at a constant rate V_0. Friction is due to both brittle and ductile contacts between the block and the rough surface. (c) Failure of brittle contacts in the model. A contact forms at position x_{0i}, and as the surfaces slide it exterts a shear stress proportional to the displacement, with stiffness γ. When the contact reaches a specified failure length a_i, it breaks and renews with a new failure length drawn from the failure length distribution.

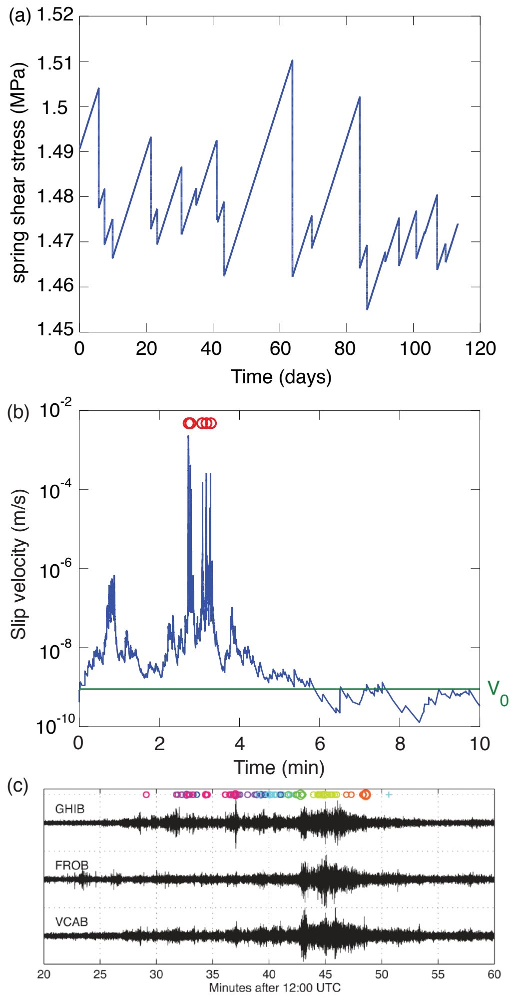

Figure 2: Plots of LFE dynamics for a brittle contact strength of 1 MPa and a ductile damping strength of $\sigma_d = 0.007$ MPa. (a) Spring shear stress as a function of time. The block undergoes stick-slip motion. (b) Slip velocity as a function of time for a single stick-slip event. The horizontal line indicates the rate at which the spring is pulled. Each stick-slip event consists of several distinct failures, denoted by circles at the top of the plot. (c) Observations of LFEs at Parkfield. The plot shows seismic waveforms at three surface stations. The circles at the top of the plot show when LFE events are detected, with different colors corresponding to LFEs at different spatial locations. During the burst of activity, there are multiple occurrences of a family within a short time period, as seen in the model. Figure taken from ref. [17].

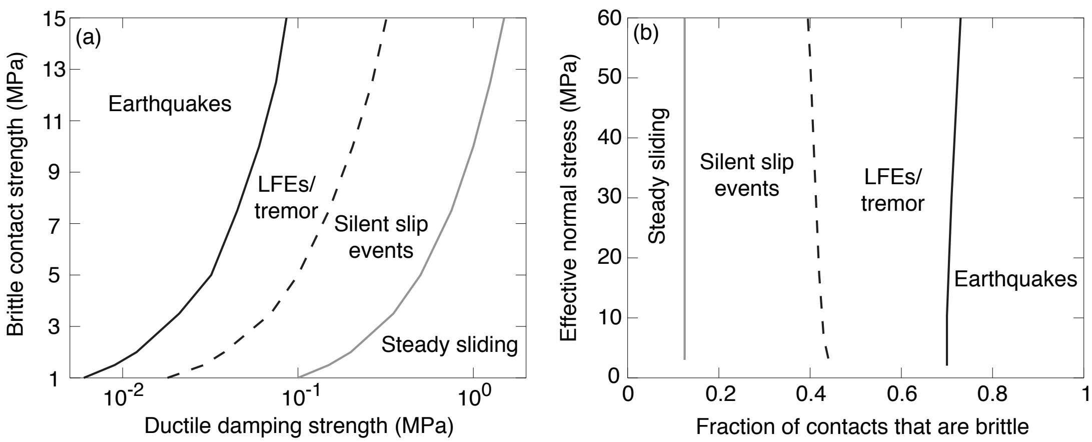

Figure 3: (a) Diagram illustrating the model dynamics as a function of the strength of the ductile damping term and the brittle contact strength. The model produces earthquakes for small values of the ductile term, and as the ductile strength increases, the model produces LFEs/tremor, silent slip, and steady sliding. At larger brittle strengths, a larger ductile damping strength is required for tremor to occur. Details of how we differentiate between regions is described in the main text. (b) Diagram illustrating model dynamics, but with the axes transformed to indicate the fraction of contacts that are brittle on the horizontal axis, and effective normal stress on the vertical axis. Tremor occurs over a range of the fraction of contacts that are brittle between 0.4-0.7, independent of the effective normal stress.

1 Supporting Online Material

In our model, we solve the equations of motion of the block slider to determine the dynamics of tremor:

$$\frac{m}{A}\frac{dV}{dt} = \Gamma\left(V_0 t - x\right) - \sum_{i=1}^{N_c}\gamma\left(x - x_{0i}\right) - \sigma_d \log\left(\frac{V + V_0}{V_0}\right) - \frac{\mu}{2c_s}V; \tag{3}$$

$$\frac{dx}{dt} = V. \tag{4}$$

Here, x is the block displacement relative to its position at $t = 0$, and V is the block velocity. The first equation is Newton's second law for the block, normalized by the fault area so that the frictional terms are in units of shear stress. The first term on the right hand side in the velocity equation is the spring shear stress, which grows linearly in time as the spring is pulled, and decreases as the block slides. The second term is the friction due to the brittle contacts, and the third term is the rate dependent ductile friction. In the model, both the brittle and ductile terms are modeled as a sum over a series of contacts. However, since the ductile strength depends only on the slip rate of the block, which does not vary among the contacts, the friction due to the ductile contacts can be expressed as a single term. The final term is radiation damping, which accounts for energy lost to seismic radiation in the earth. Parameters include the mass per unit area of the block m/A, the spring stiffness per unit area Γ, the long-term creep velocity on the fault V_0, the number of brittle contacts N_c, the stiffness per unit area of individual brittle contacts γ, the reference position of each contact x_{0i}, the ductile damping strength σ_d, and the radiation damping coefficient $\mu/(2c_s)$, where μ is the shear modulus and c_s is the

Table 1: Parameter values.

Parameter	Description
$m/A = 3$ MPa s^2/m	Mass per unit of contact area of the block
$\Gamma = 30$ MPa/m	Spring stiffness per unit area
$V_0 = 30$ mm/yr	Long term driving rate
$N_c = 1000$	Number of brittle contacts
$\mu = 30$ GPa	Shear modulus
$c_s = 3$ km/s	Shear wave speed
$a_{\min} = 1$ μm	Minimum contact failure length
$a_{\max} = 20$ μm	Maximum contact failure length
$\gamma =$ varies	Brittle contact stiffness
$\sigma_d =$ varies	Ductile damping strength

shear wave speed. Each contact also has a failure length a_i, which is drawn from the distribution $p_0(a) \propto a^{-2}$, with minimum and maximum lengths $a_{\min}$ and $a_{\max}$, respectively. Parameter values are given in Table 1.

In the friction model, we make several simplifying assumptions. For the brittle contacts, we assume that the stiffness of all contacts is the same. Real frictional contacts have varying sizes and shapes, and thus could have different stiffnesses. However, in the model the failure distance is different for each contact, so every contact will have a different failure stress even though the stiffness is the same for all contacts. For the ductile term, the logarithmic velocity dependence in the ductile term is problematic at $V = 0$, and is regularized by adding a cutoff velocity, chosen to be the long term driving rate. This sets the ductile damping to zero when the block is not slipping. We also make the simplifying assumption that every contact has the same damping strength σ_d. Since we model a single family of tremor at one spatial location, this assumption implies that the ductile damping strength does not vary rapidly with spatial position, and is roughly constant for a given family. More complex models that take into account the variations of ductility among different families could be constructed, but is beyond the scope of this paper.

To integrate the equation of motion for the block slider, we first change variables from x to $u = x - (\Gamma V_0 t)/(\Gamma + N_c\gamma)$. This change of variables removes the explicit appearance of time in the equations of motion, and improves the numerical efficiency by allowing for larger time steps between failure events. Written in terms of u, the equations of motion are

$$\frac{m}{A}\frac{dV}{dt} = -\left(\Gamma + N_c\gamma\right)u + \sum_{i=1}^{N_c}\gamma x_{0i} - \sigma_d \log\left(\frac{V+V_0}{V_0}\right) - \frac{\mu}{2c_s}V; \tag{5}$$

$$\frac{du}{dt} = V - \frac{\Gamma V_0}{\Gamma + N_c\gamma}, \tag{6}$$

We require that no back slip occurs (i.e. $V \geq 0$); if the velocity drops below zero, we set the block velocity to zero until the spring stretches enough to overcome the brittle contact friction.

Parameters can be made dimensionless by rescaling all times by the unimpeded mass/spring oscillation time ($\sqrt{m/(A\Gamma)}$) and rescaling all lengths by the maximum contact failure distance $a_{\max}$. This leaves the following dimensionless parameters: the scaled brittle contact stiffness γ/Γ, the scaled ductile damping strength $\sigma_d/(\Gamma a_{\max})$, the scaled driving rate $V_0\sqrt{m/(A\Gamma)}/a_{\max}$, the scaled radiation damping coefficient $\mu/(2c_s)\sqrt{A/(\Gamma m)}$, and the minimum contact failure distance $a_{\min}/a_{\max}$. Because the brittle and ductile strengths are poorly constrained in the earth, we fix the other parameters and focus on how the brittle and ductile strengths affect the slider dynamics.

At the end of each time step, we check if the contact population must be updated. In the model, every brittle contact has a reference position x_{0i} and a failure length a_i, and the contact fails if $x > x_{0i} + a_i$. When a contact breaks, its reference length x_{0i} is reset to the current value of x and a new value for a_i is chosen from the distribution $p_0(a)$.

Because the equations of motion for the block are quite stiff, we integrate using a linearly implicit trapezoidal method that is second order accurate in time. We use an adaptive time step method, which allows for sufficient resolution of failure events while taking large time steps between events for maximum efficiency.

To constrain the *in situ* conditions for the LFEs, we estimate a lower bound on the slip rate during failure. For LFEs with a recurrence time of 3 days, and a long term slip rate of 30 mm/yr, each event accumulates approximately 100 μm of slip. Because significant energy in the seismic data is above 10 Hz, an estimate for the duration of slip is 0.1 s. The slip rate during LFEs at Parkfield is then roughly (100 μm)/(0.1 s) = 10^{-3} m/s. However, it is possible that not all of the slip accumulates during tremor, so the slip during an individual event could be lower. Therefore, we use a lower bound of 10^{-4} m/s on the slip rate in the ~ 3 day recurrence events. This allows us to determine the brittle and ductile strengths that produce slip rates of this magnitude.

To estimate the conditions required for this slip to be detectable seismically, we assume that tremor can be treated as a point source. If the observation point is in the far field, then a point source produces a surface displacement u_{surf} [1]

$$u_{surf} \sim \frac{1}{4\pi r \rho c_s^3} \frac{dM_0}{dt}, \tag{7}$$

where dM_0/dt is the moment rate, r is the distance to the observation point, ρ is density, and c_s is shear wave speed. This estimate is for shear waves, as the compressional wave displacement is smaller. Observations of tremor magnitude report peak ground velocity (PGV) [2], the maximum particle velocity at the surface. Thus, we differentiate to obtain

$$v_{surf} \sim \frac{1}{4\pi r \rho c_s^3} \frac{d^2 M_0}{dt^2}. \tag{8}$$

Because this is an order of magnitude estimate, we neglect attenuation, which should not significantly affect the results at the observation distance at Parkfield.

The minimum PGV at Parkfield is $\sim 10^{-9}$ m/s and r should be around 25 km [12], giving a moment acceleration estimate of $d^2M_0/dt^2 \sim 10^{10}$ Nm/s^2, assuming $c_s = 3$ km/s and $\rho = 3$ g/cm^3. Assuming a shear modulus of 30 GPa, the product of the slip acceleration and the slipping area is then 1 m^3/s^2. Given our slip rate estimate of 10^{-3} m/s and a duration of 0.1 s, the corresponding slip acceleration estimate is 10^{-2} m/s^2. Slip with this acceleration is detectable as long as the slipping area is at least (10 m)^2. This implies that tremor consists of small $\sim$ (10 m)^2 patches on the fault with semi-brittle frictional characteristics at depth. The patches are part of a larger area of the fault that corresponds to a particular family of LFEs. In our model, the entire block represents the full area of a single family, while individual collections of frictional asperity contacts are the individual small patches that fail in a single LFE.

References

[1] K. Aki, P. G. Richards, *Quantitative Seismology* (Univ. Science Books, Sausalito, CA, 2002).

[2] D. R. Shelly, J. L. Hardebeck, Precise tremor source locations and amplitude variations along the lower-crustal central San Andreas Fault. *Geophys. Res. Lett.* **37**, L14301 (2010).